AAS 24-164

SHORT-TERM LOITERING IN THE VICINITY OF THE GATEWAY NEAR RECTILINEAR HALO ORBIT IN THE CIRCULAR RESTRICTED THREE-BODY PROBLEM

Lorin Nugent[*], Matthew Bolliger[†], Aurélie Héritier[‡], Diane Davis[§], Kathleen Howell[¶]

The NASA Gateway spacecraft is intended to frequently host visiting vehicles in support of the Artemis program and cislunar operations. Relative motion in libration point orbits such as the Gateway Near Rectilinear Halo Orbit (NRHO) is an area of ongoing research, and the rendezvous, proximity operations, and docking procedures in this challenging environment are under development. This paper presents a preliminary investigation into potential strategies for short-term spacecraft loitering in the vicinity of the NRHO prior to rendezvous or departure. Four methods are introduced and evaluated within the Circular Restricted Three-Body Problem to assess their ability to minimize the relative drift of the visiting spacecraft during the loitering phase. Two operational cases are evaluated and the results are summarized for each strategy as well as some general observations regarding proximity operations in the NRHO.

INTRODUCTION

With an increased global focus on missions to the lunar region in the next decade, cislunar space is expected to become a busy hub for a broad range of mission applications. Dozens of international missions are expected to launch to cislunar space by 2030, with objectives spanning science, defense, and commercial development.[1] Leading the human exploration side is the NASA-led Artemis program, an international collaboration aiming to establish a permanent and sustainable human presence on the Moon. The NASA Gateway spacecraft is planned to occupy a multi-body orbit that repeatedly passes close to the Moon, i.e., a Near Rectilinear Halo Orbit (NRHO).[2] It is intended to serve as a crewed outpost in support of the Artemis program and as a staging point for eventual translunar and deep space departures. As such, the Gateway station is expected to frequently host crewed spacecraft such as Orion and Starship, resupply modules, service modules, and other visiting vehicles.

The examination of relative motion between space objects is relevant to multiple key mission elements. Orbit stationkeeping, collision avoidance, and spacecraft transfers are a few notable examples of relative behaviors that frequently appear in the mission design and maintenance process. The dynamical complexities of the Gateway orbital regime complicate relative behavior, leading to numerous ongoing investigations for operations pertaining to Artemis and Gateway.[3–5] Spacecraft rendezvous, proximity operations, and docking (RPOD) procedures for libration point orbits also necessarily differ from the operations established for the International Space Station and other Keplerian rendezvous scenarios due to the differences in the operational regimes. The current investigation seeks to contribute to the understanding of efficient spacecraft proximity operations for vehicles docking with the Lunar Gateway. The focus of this analysis is to explore some of the options available for visiting spacecraft to efficiently loiter in the vicinity of the NRHO prior to Gateway rendezvous or departure.

[*]Astrodynamics Engineer Intern, Advanced Space LLC, nugentl@purdue.edu.
[†]Astrodynamics and Satellite Navigation Engineer, Advanced Space LLC, matt.bolliger@advancedspace.com.
[‡]Principal Astrodynamics and Satellite Navigation Engineer, Advanced Space LLC, aurelie.heritier@advancedspace.com.
[§]Gateway Mission Design Lead, Johnson Space Center, Houston TX, diane.c.davis@nasa.gov.
[¶]Hsu Lo Distinguished Professor, School of Aeronautics and Astronautics, Purdue University, howell@purdue.edu.

BACKGROUND

Spacecraft rendezvous is integral to space technology development. It is a capability already demonstrated extensively in Keplerian orbits, enabling on-orbit assembly of large vehicles, crew transits, satellite servicing, and orbital refueling. The success of these efforts is due to a strong understanding of relative two-body dynamics. In 1960, Clohessy and Wiltshire published a solution to the linearized equations of relative motion for spacecraft in an Earth circular orbit.[6] The formulation assumes an unperturbed, circular orbit for a target spacecraft with a second vehicle in its vicinity, and is a reasonable approximation for small distances between the two spacecraft. The Clohessy-Wiltshire equations are foundational to the development of many modern spacecraft rendezvous control strategies.[7] However, the equations are dependent on the fact that the underlying circular orbit possesses an analytical description, which is not the case for trajectories in the n-body problem.

While spacecraft rendezvous in multi-body orbits draws much recent attention, formation flight in this regime is not a new topic; investigations appear over multiple decades. Early considerations for formation flight examine the center invariant manifold of periodic orbits and quasi-periodic trajectories for bounded, long-term natural behaviors.[8,9] Other authors employ control techniques to actively maintain formations or modify the natural rotational frequency of the local dynamics.[10–12] Within the past decade, additional focus is given to the reformulation and analysis of relative equations of motion in more convenient reference frames,[13,14] as well as leveraging differential corrections for the determination of repeating trajectories in a relative frame.[15] Analysis presented in the context of formation flight for libration point orbits is inherently relevant to spacecraft RPOD in a similar dynamical environment. Much of the work in this investigation builds on prior contributions to the study of formation flight.

DYNAMICAL MODEL

The Circular Restricted Three-Body Problem (CR3BP) is employed as the dynamical model to represent spacecraft motion on or near the Gateway NRHO for the current investigation. In the CR3BP, the mass of a spacecraft P_3 is infinitesimal compared to the masses of the primary bodies P_1 (the larger primary, e.g., Earth) and P_2 (the smaller primary, e.g., Moon), that exist as an isolated two-body problem. The primaries orbit their mutual barycenter on closed conics, which are assumed circular. The barycenter B is the origin for a coordinate frame that rotates with the mean motion of the primary orbits such that $\hat{x}$ always points from P_1 to P_2, $\hat{z}$ points in the direction of the orbital angular momentum of the primaries, and $\hat{y}$ completes the dextral orthonormal triad as illustrated in Figure 1.

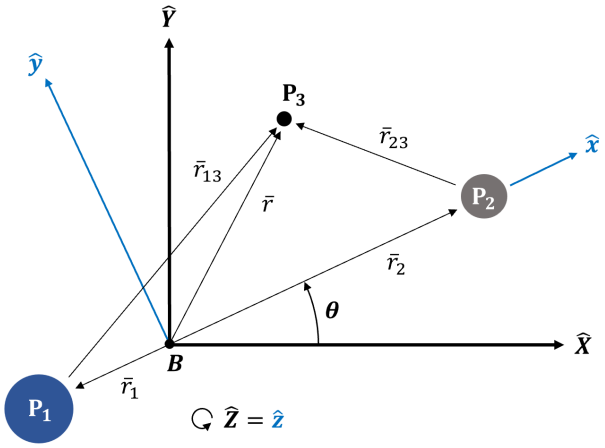

Figure 1: The CR3BP rotating frame and arbitrary inertial frame.

The equations of motion are expressed in nondimensional form to maintain generality and reduce error

during numerical propagation. The terms (x, y, z) and $(\dot{x}, \dot{y}, \dot{z})$ are used to represent the nondimensional position and velocity coordinates, respectively, of P_3 relative to the barycenter as viewed in the rotating frame. The characteristic length (l^*) is the distance between the primaries, characteristic mass (m^*) is defined as the sum of the primary masses, and characteristic time (t^*) is selected such that the mean motion of the primaries $\dot{\theta}$ is equal to 1. The mass ratio μ is defined as the mass of the second primary m_2 divided by the characteristic mass m^*, and is a defining characteristic of the system dynamics. With this formulation, the equations of motion are written in nondimensional rotating coordinates as

$$\ddot{x} = 2\dot{y} + \frac{\partial U^*}{\partial x}, \qquad \ddot{y} = -2\dot{x} + \frac{\partial U^*}{\partial y}, \qquad \ddot{z} = \frac{\partial U^*}{\partial z} \tag{1}$$

where U^* is the pseudopotential function, defined

$$U^* = \frac{1-\mu}{r_{13}} + \frac{\mu}{r_{23}} + \frac{1}{2}(x^2 + y^2) \tag{2}$$

Five equilibrium points, the Lagrange points or libration points, exist in the CR3BP model, denoted as L_i for $i = 1, ..., 5$. The CR3BP equations of motion possess one known integral, an energy-like quantity called the Jacobi Constant. This integral is defined and determined to be expressed as $C = 2U^* - v^2$, where v is the nondimensional velocity magnitude as it appears in the rotating frame.

MOTIVATION BEHIND LOITERING STRATEGIES

Four potential loitering strategies are investigated. Two stem from prior literature on formation flying configurations in Sun-Earth libration point orbits, leveraging information regarding the local acceleration and linearization information near a state on a reference orbit. The third strategy uses invariant manifold structures to maintain long-term, bounded trajectories in the vicinity of the periodic orbit. The last strategy also leverages linearized dynamics, but for an arbitrary segment of the reference orbit instead of a single location. The background for each method is presented in this section.

Drift Regions

One application for spacecraft formation flight is the scientific observations of distant star systems. Multiple missions have been proposed that implement an orbiting telescope with a separate occulter spacecraft between the telescope and a distant star to block out the star light in search of exoplanets.[16,17] Given a telescope in a libration point orbit, Héritier and Howell investigate the dynamics in the Sun-Earth system to determine regions along the reference path where the spacecraft temporarily maintain loose ballistic formations.[18] There exist many parallels to the current investigation and this work forms the basis of two implemented loitering strategies.

Consistent with terminology from the literature, the primary vehicle of interest (e.g., the telescope or Gateway) is termed the "chief" spacecraft. A secondary spacecraft (e.g., the occulter or a visiting vehicle) is termed a "deputy" spacecraft. For the application investigated by Héritier and Howell, the goal is efficient maintenance of the deputy spacecraft at a constant position relative to the chief spacecraft during science collection. The authors identify two methods to isolate natural dynamical regions that may be suitable for a deputy spacecraft. The first, determined empirically, evaluates the magnitude of relative accelerations of states that are offset slightly in position from the chief spacecraft, assumed to be precisely on the reference orbit. A spherical shell of discrete points is initialized surrounding the chief location and assigned the same absolute velocity as the chief. The new absolute acceleration vector of each point is then determined from the equations of motion, subtracted from the chief acceleration, and the resulting relative acceleration vector magnitude is used as a metric to represent the potential for deputy spacecraft to drift from that location. This information is visualized for a chief state at apolune along the Gateway NRHO in Figure 2. Points along the sphere with the lowest relative acceleration magnitudes are denoted "low drift regions". For additional

clarity in the explanation of loitering strategy implementation, the "medium" and "high" drift regions are also denoted in the figure.

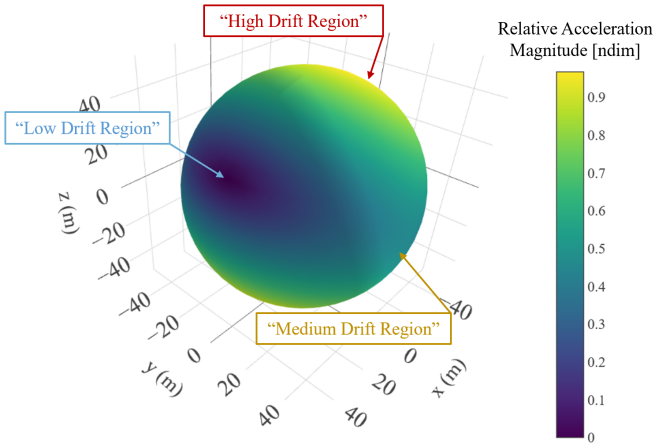

Figure 2: Discretized sphere color-coded by relative acceleration magnitude.

Relative Acceleration Ellipsoid

The second method captures similar information with a semi-analytic approach from Héritier and Howell,[18] leveraging the first-order variational equations. Written in matrix form, the relationship between variations in position and acceleration (assuming $\delta\dot{\bar{r}} = \bar{0}$) appears in the form

$$\delta\ddot{\bar{r}} = \begin{bmatrix} U^*_{xx} & U^*_{xy} & U^*_{xz} \\ U^*_{yx} & U^*_{yy} & U^*_{yz} \\ U^*_{zx} & U^*_{zy} & U^*_{zz} \end{bmatrix} \delta\bar{r} = \tilde{U}\delta\bar{r} \tag{3}$$

The terms U^*_{ij} denote the ij-second partial derivatives of the pseudopotential function U^* (provided in Eq. (2)). The goal is the determination of regions near the reference trajectory where the magnitude of the relative acceleration vector ($|\delta\ddot{\bar{r}}| = \delta\ddot{\bar{r}} \cdot \delta\ddot{\bar{r}}$) is zero so that a relative position may naturally persist. However, since the relative acceleration never precisely equals zero, in practice, a maximum acceleration magnitude threshold ϵ is selected. If ϵ is defined as the upper threshold of relative acceleration magnitude, then

$$\delta\bar{r}^T \tilde{U}^T \tilde{U} \delta\bar{r} \leq \epsilon \tag{4}$$

By transforming Eq. (4) to canonical form and introducing a change of coordinates, the authors demonstrate that the solution appears as a quadratic surface. The principal axes of this surface are the eigenvectors of $\tilde{U}$, with coordinate y_i in the $\bar{V}_i$ eigenvector direction, i.e.,

$$\lambda_1^2 y_1^2 + \lambda_2^2 y_2^2 + \lambda_3^2 y_3^2 \leq \epsilon \tag{5}$$

For the cases presented by Héritier and Howell, as well as in the current investigation, these quadratic surfaces are ellipsoids. Figure 3 provides a scaled visualization of these ellipsoids at various points along a Sun-Earth L_2 halo.[18] Note that the size and orientation of the surfaces change depending on the local dynamics.

Through the analysis of two Sun-Earth L_2 halo orbits, Héritier and Howell identified natural dynamical regions that reduce the control inputs required to maintain precise formations for scientific observations. While the motivation is different, the desired behavior for the deputy spacecraft is precisely the same as in

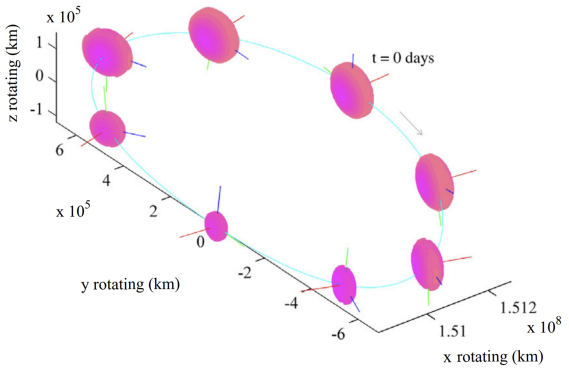

Figure 3: "Zero" relative acceleration ellipsoids.[18]

the loitering case. Both applications share the common goal of uncovering natural dynamical structures in the vicinity of multi-body orbits to maintain formations of spacecraft without strict requirements on their relative configuration. As such, both the empirical and semi-analytic methodologies are potentially applicable to the Gateway orbital environment for short-term loitering. There are, however, important differences between the employment of these strategies in the literature and the present RPOD investigation. The Earth-Moon system operates on shorter timescales and distances than the Sun-Earth system. Formations that maintained their geometry for many days in a Sun-Earth halo orbit may only be reasonable for a few hours and smaller spacecraft separations in an Earth-Moon halo of similar geometry. Additionally, neither of the halo orbits assessed in the literature possess a close pass to the smaller primary, avoiding much of the nonlinear effects characteristic of perilune passage in the Gateway NRHO. To perform scientific observations of distant star systems, identifying formations in an inertial frame is beneficial. Deputy spacecraft loitering configurations are expected to be maintained in a rotating frame.

Complex Center Manifold

Quasi-periodic orbits (QPOs) exist in the vicinity of periodic orbits and are typically constructed from a monodromy matrix that yields at least one pair of complex center eigenvalues.[19] Families of QPOs form invariant tori that evolve from the periodic orbit. Early investigation into quasi-periodic behavior implement semi-analytical constructions based on the governing dynamics. Farquhar and Kamel use a Lindstedt-Poincaré strategy to approximate QPOs in the cislunar regime.[20] Gómez et al. employ similar approaches to construct quasi-halo orbits in the CR3BP.[21] Leveraging information from the semi-analytical methods of previous authors, Howell and Pernicka develop numerical techniques to correct approximations to converge Lissajous trajectories for an arbitrary number of revolutions with CR3BP nonlinear effects.[9] Significant developments in computing technology lead to further advances in numerical techniques. More recent efforts on QPOs focus on direct methods to compute invariant tori.[22] This natural, bounded motion surrounding a periodic orbit is suitable to long-term spacecraft formations. Early considerations of QPOs within the context of formation flying first appear in 1998.[8] In subsequent years, formation flying applications of QPOs are further examined and validated much more extensively.[23,24] In the context of RPOD for Artemis, the existence of a complex center invariant manifold associated with the Gateway orbit opens opportunities to leverage quasi-periodic structures for spacecraft loitering or formation flight.

A first-order approximation for the invariant curve relative a fixed point is determined by leveraging stroboscopic mapping techniques. Using a modified version of Eq. (3.6) from McCarthy,[19] states are approximated on the invariant curve of the complex center manifold. The term $\bar{x}^*$ is a fixed point on the orbit, $\bar{u}_i \triangleq \text{Re}[\bar{v}_c]\cos\theta_i - \text{Im}[\bar{v}_c]\sin\theta_i$, where $\bar{v}_c$ is one of the complex center eigenvectors from the monodromy matrix for the orbit, and $\alpha = d/l^*$ is the step-off distance nondimensionalized by the characteristic length of the primary system, i.e.,

$$\bar{x}_i = \bar{x}^* + \alpha \left(\frac{\bar{u}_i}{(u_x^2 + u_y^2 + u_z^2)^{\frac{1}{2}}} \right) \tag{6}$$

Values for θ_i are selected to approximate multiple points that lie on the invariant curve. The equation is formulated such that deputy states are easily initialized at a consistent distance from the chief.

In practice, Eq. (6) is only the first step to obtaining a corrected quasi-periodic trajectory within the nonlinear dynamics. However, the uncorrected, linear approximation of quasi-NRHO initial states is deemed appropriate for the short-term behavior in the current RPOD investigation. Deputy states are initialized at most 5 kilometers away from the periodic orbit near apolune, where the linear approximation is most accurate. Additionally, the NRHO is nearly stable in a linear sense, meaning that errors in the nonlinear state do not quickly diverge toward the unstable invariant manifold. Figure 4 shows a linear approximation of the quasi-NRHO evaluated via propagation of the linear variational equations, where each color represents an individual trajectory. When compared to nonlinear propagation of the same initial states for a 5 kilometer step-off, the maximum error of the linear approximation is under one meter until perilune, where it spikes to at most 150 meters before returning to similarly low values.

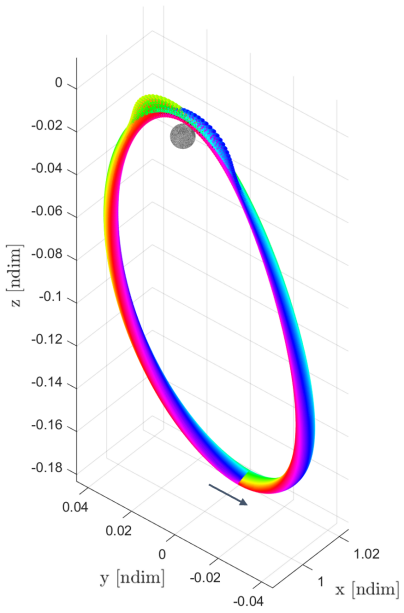

Figure 4: Linear approximation of quasi-NRHO states.

Stretching/Restoring Directions

Stretching and restoring directions describe the principal directions for expansion or contraction of phase space in the vicinity of a reference trajectory.[25] They are determined using the state transition matrix (STM) $\Phi(t_f, t_0)$ or the Cauchy Green Tensor (CGT) $\mathbb{C}(t_f, t_0) = \Phi(t_f, t_0)^{\mathrm{T}}\Phi(t_f, t_0)$, each providing related but slightly different information. Short et al. employ the CGT with the theory of hyperbolic Lagrangian coherent structures to determine low-cost transfers within a higher-fidelity force model.[26] The authors accomplish this task by identifying dynamical structures with finite time Lyapunov exponent maps for cases where invariant manifolds and other time-autonomous dynamical structures are not as accessible. Within the context of the CR3BP, stretching and restoring directions are useful for determining more efficient departure and/or arrival transfer options for orbits that are stable or nearly stable.[27] Many prior investigations have leveraged the maximum stretching direction, in forward time for departures or reverse time for arrivals.

For a spacecraft loitering application, a priority is given to minimizing the relative drift of the deputy spacecraft. These loitering regions may differ from the chief state in both position and velocity as necessary to minimize drift. By isolating the 3×6 $\phi_{r,rv}$ submatrix of the reference STM, the impact of initial position and velocity changes are mapped to changes in final position only.

$$\phi_{r,rv} = \begin{bmatrix} \phi_{r,r} & \phi_{r,v} \end{bmatrix} \tag{7}$$

Note that the STM is always tied to a time horizon $t_h = t_f - t_0$. The time horizon for the reference STM is the desired deputy loitering time. Following the nomenclature from Muralidharan,[25] $\phi_{r,rv}$ is rewritten in terms of its Singular Value Decomposition (SVD). The matrix Σ is 3×6 with the singular values $\sigma_1 > \sigma_2 > \sigma_3$ as its main diagonal and zeros for all other elements. The columns of the 6×6 matrix $\mathbb{V}$ are the 6D orthonormal stretching/restoring directions at t_0, where $\bar{V}_i$ corresponds to the singular value σ_i for $i = 1, 2, 3$. Similarly, the columns of the 3×3 matrix $\mathbb{U}$ are the 3D (position) orthonormal stretching/restoring directions at t_f, with $\bar{U}_i$ corresponding to the singular value σ_i.

$$\mathbb{U}\Sigma\mathbb{V}^* = \phi_{r,rv}(t_f, t_0) \tag{8}$$

A 2D representation is depicted in Figure 5, illustrating the mapping of stretching/restoring directions from the initial to final time through the CGT.[27] A perturbation in the $\bar{V}_i$ direction is rotated to the $\bar{U}_i$ direction and scaled by a factor σ_i.

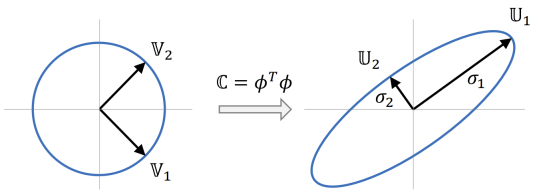

Figure 5: Principal stretching and restoring directions.[27]

The singular values σ_i represent the scaling factors in the linear mapping. Since the STM maps perturbations in position and/or velocity, the singular values reflect perturbation growth or contraction along the reference trajectory. For a position-to-position mapping, this value would represent the ratio of distances at the initial and final times. However, for the mixed-phase case that is represented by $\phi_{r,rv}$, the result is more difficult to interpret. Capturing the significance of this ratio for the positional offset versus the velocity offset is not as clear.

For the purpose of spacecraft loitering, it is desirable to maintain a distance ratio $\delta r_f/\delta r_0$ equal to 1 between the initial and final times. Information from the SVD of $\phi_{r,rv}$ is leveraged to derive a relationship that predicts the ratio $\delta r_f/\delta r_0$ when the initial state perturbation is one of the 6D $\bar{V}_i$ directions. Begin by expressing the definition of the singular value in terms of the state perturbations at the initial and final times, i.e.,

$$\sigma_i = \frac{|\delta\bar{x}_f|}{|\delta\bar{x}_0|} = \frac{(\delta x_f^2 + \delta y_f^2 + \delta z_f^2)^{\frac{1}{2}}}{(\delta x_0^2 + \delta y_0^2 + \delta z_0^2 + \delta\dot{x}_0^2 + \delta\dot{y}_0^2 + \delta\dot{z}_0^2)^{\frac{1}{2}}} \tag{9}$$

Recognizing that $\delta r^2 = \delta x^2 + \delta y^2 + \delta z^2$ and $\delta v^2 = \delta\dot{x}^2 + \delta\dot{y}^2 + \delta\dot{z}^2$, both sides of the equation are squared and rewritten in the form

$$\sigma_i^2 = \frac{\delta r_f^2}{\delta r_0^2 + \delta v_0^2} \tag{10}$$

The right side of Eq. (10) is now multiplied by the quantity $\delta r_0^2/\delta r_0^2 = 1$ to yield

$$\sigma_i^2 = \frac{\delta r_f^2/\delta r_0^2}{1 + \delta v_0^2/\delta r_0^2} \tag{11}$$

Finally, terms are rearranged to isolate the desired ratio $\delta r_f/\delta r_0$.

$$\frac{\delta r_f}{\delta r_0} = \sigma_i \left[1 + \left(\frac{\delta v_0}{\delta r_0}\right)^2\right]^{\frac{1}{2}} \tag{12}$$

Note that the ratio $\delta v_0/\delta r_0$ is given by the relative magnitudes of the position and velocity components of $\bar{V}_i$. The relationship in Eq. (12) predicts the distance ratio between the initial and final time for a state perturbed from the reference orbit in both position and velocity along the $\bar{V}_i$ singular vector. It is dependent only on information from the SVD of the corresponding STM submatrix $\phi_{r,rv}(t_f, t_0)$.

REFERENCE ORBIT

The NASA Gateway is planned to reside in an Earth-Moon 9:2 synodic NRHO, a member of the L_2 southern halo family. The orbit is visualized in the CR3BP rotating frame in Figure 6. This particular orbit was selected, in part, for its constant line-of-sight to the Earth, extended intervals of lunar south pole visibility, stability characteristics, and eclipse avoidance properties.[28] The simplest dynamical model effective for constructing such an orbit must include the gravitational influences of both the Earth and the Moon. While periodic in the CR3BP, the NRHO does not possess a convenient analytical description, in contrast to the Keplerian-type orbits that exist in the relative two body problem. The 9:2 NRHO is symmetric across the x-z plane, with a period of approximately six and a half days, consistent with its designed resonance ratio. The orbital perilune and apolune are roughly 3,000 km and 70,000 km, respectively, from the center of the Moon. The following parameters are employed to model the Earth-Moon CR3BP system: mass ratio $\mu = 0.012150584270$, characteristic length $l^* = 384{,}400$ km, characteristic time $t^* = 3.751902619517e5$ seconds. The nondimensional initial conditions for the orbit are $(x, y, z, \dot{x}, \dot{y}, \dot{z}) = (1.022023976774, 0, -0.182098475077, 0, -0.103261718478, 0)$, with a nondimensional period of 1.511143593137. Propagating these initial conditions with relative and absolute tolerances of 1e-10 results in an error in final 6D state on the same order of magnitude as the integration tolerance.

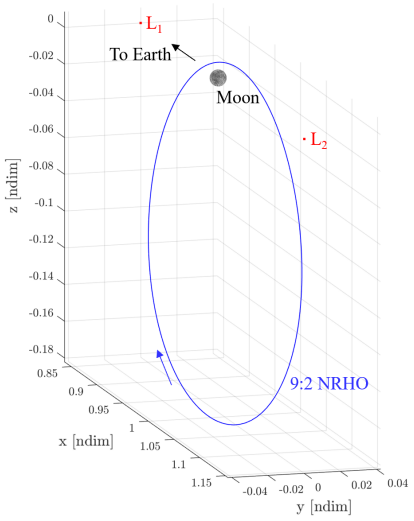

Figure 6: The 9:2 synodic NRHO in the CR3BP rotating frame.

LOITERING STRATEGY DEFINITIONS

Four different strategies are examined to assess their application for short-term loitering near Gateway prior to arrival or departure. After selecting an initial state for the chief spacecraft along the reference orbit, a separation distance, and loitering time horizon, deputy states are initialized as described for each of the following schemes:

- **Drift Regions (DR)**: - Regions of low drift are determined empirically from the relative acceleration magnitudes of states on a sphere with a radius equal to the selected loitering separation distance from the chief spacecraft. Deputy states are initialized in a ring surrounding the chief in the plane containing the low and medium drift regions, normal to the high drift region as depicted in Figure 2. n deputy states are assigned the chief spacecraft velocity vector.
- **Relative Acceleration Ellipsoid (RAE)**: An ellipsoid of constant relative acceleration magnitude (ϵ) is computed using Eq. (5). For the current investigation, the value of ϵ is selected to be 10% of the difference between lowest and highest relative acceleration magnitudes determined from the discretized sphere. n deputy states are initialized at locations on this ellipsoid that lie at the desired loitering distance from the chief. Deputy states are assigned the chief spacecraft velocity vector.
- **Complex Center Manifold (CCM)**: n deputy spacecraft are initialized along the linear approximation for the invariant curve of the complex center manifold, using the relationship in Eq. (6). Deputy states differ from the chief in both position and velocity.
- **Stretching/Restoring Directions (SRD)**: The STM is evaluated along the reference orbit for the selected loitering time horizon. The SVD of the $\Phi_{r,rv}$ submatrix is evaluated to determine the singular vector that corresponds to a position offset ratio closest to 1, as described in Eq. (12). Two deputy spacecraft are initialized, in the positive and negative singular vector directions relative to the chief. Deputy states differ from the chief in both position and velocity.

Of the four defined strategies, the DR and RAE methods employ changes in only position relative to the chief, while both the position and velocity vectors are adjusted for CCM and SRD states.

SCENARIO FOR INVESTIGATION

To simulate proximity operations, deputy spacecraft states are initialized in the vicinity of the chief and their trajectories are allowed to evolve ballistically under the CR3BP equations of motion given by Eq. (1). Two cases are considered for short-term loitering:

- **Case 1** The distance between the chief and deputy spacecraft is set at **50 meters**. Deputy spacecraft loiter for **4 hours** prior to rendezvous or departure.
- **Case 2** The distance between the chief and deputy spacecraft is set at **5 kilometers**. Deputy spacecraft loiter for **24 hours** prior to rendezvous or departure.

These cases are defined to capture potential operational limitations on visiting spacecraft due to high traffic and limited docking ports on the Gateway station. Six deputy spacecraft are simulated for each identified strategy other than the SRD method, for which only two are simulated due to limitations within the formulation of the strategy. This number was selected as a representative upper bound on vehicles expected to be in a short-term loitering configuration for this preliminary feasibility analysis.

Of equal importance to defining deputy spacecraft loitering strategies relative to a chief state is the identification of locations on the underlying orbit where proximity operations may be conducted most efficiently. Prior analysis has shown that first-order linear approximations of the dynamics yield considerably higher accuracy near apolune than perilune, which is more sensitive to small state errors. Consistent with Keplerian orbits, orbital speeds are significantly slower near apolune, an attribute that is beneficial to proximity operations. Location information along the NRHO is defined via the chief spacecraft instantaneous osculating true anomaly (TA), for which perilune is defined at 0 degrees. While other methods such as orbit encoding may be more appropriate for multi-body orbits,[29] osculating true anomaly values are chosen to be consistent with Gateway stationkeeping literature. True anomalies of 160 and 200 degrees are identified as favorable locations to conduct orbit maintenance burns.[3] To capture these locations as well as the intermediate region containing apolune, a domain of chief spacecraft starting TAs is selected as 150 to 210 degrees. Chief spacecraft states at each integer degree of TA within this range are taken as the starting location for loitering simulations in each of the defined cases. All simulations are performed in Python using the default Runge-Kutta-Fehlberg integration scheme and integration tolerances of 1e-10.

PERFORMANCE METRICS

The performance of each loitering strategy is assessed using five metrics that aid in the comparison of the spacecraft relative motion. These performance metrics are termed ‘total drift’, ‘in-line drift’, ‘transverse drift’, ‘range to chief’, and ‘range to nearest deputy’, and each is assessed from relative states in the rotating frame. Total drift is defined as the magnitude of the difference between a current deputy relative position and its relative position at the start of the loitering period. Total drift is also broken down into two sub-categories – in-line drift, which is the component of total drift in the direction of the deputy spacecraft’s original relative position, and transverse drift, which is the magnitude of remaining spatial position offset perpendicular to the in-line drift direction. The range to chief is the magnitude of the instantaneous relative position vector, and the range to nearest deputy is the distance between the two closest deputy spacecraft for a given loitering strategy. These performance metrics are depicted in Figure 7. Note that all metrics are shown as planar in the figure but are spatial in practice.

CASE 1 RESULTS

This section summarizes the loitering performance trends for Case 1, the shorter of the two operational test cases. For each integer TA in the domain 150 to 210, deputy spacecraft states are defined 50 meters from

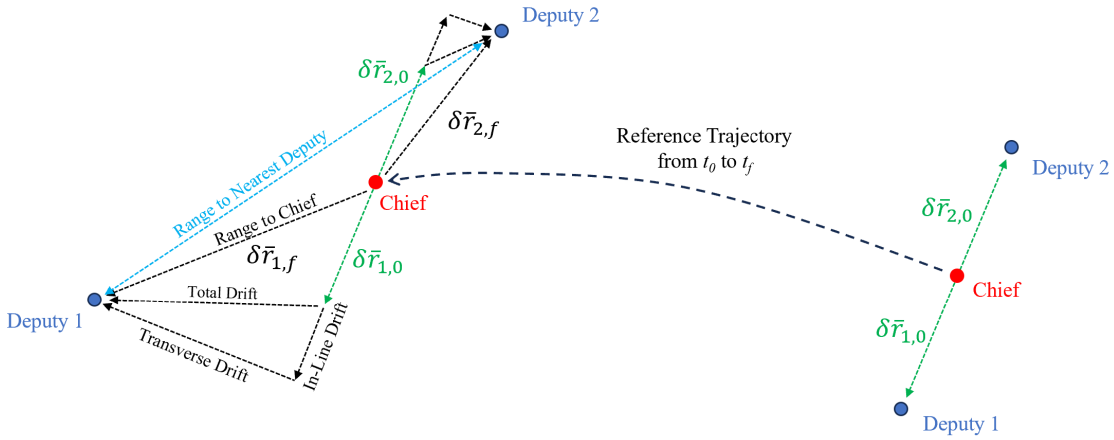

Figure 7: Loitering strategy performance metrics.

the chief as described in the Loitering Strategy Definitions and are simulated alongside the chief spacecraft states for 4 hours. The performance metrics are then evaluated from relative states of each deputy spacecraft throughout the propagation time. Sample outputs are provided for a starting TA of 170 degrees (ending at a TA of 171.82 degrees after 4 hours), which is selected as a representative case to illustrate some of the primary results.

It is worth first observing the starting positions that the deputy spacecraft occupy based on their definitions. Figure 8 shows the starting locations of each deputy spacecraft (denoted as circular markers) in a chief-centered rotating frame. For reference, a sphere color-coded by relative acceleration magnitude is included to better understand the local dynamics, where states on the sphere have no velocity relative to the chief, which rests at the center. As is seen in Figure 8, DR, RAE, and SRD states tend to cluster near the plane containing the low and medium drift regions. The CCM states all exist in a plane as defined in Eq. (6), however the orientation of this plane in position space varies drastically along the orbit and does not correlate to the other methods. While DR and RAE states are defined differently, the intersection of the ellipsoid from the RAE method with the sphere from the DR method is essentially equivalent to a contour line of constant relative acceleration magnitude on the sphere. Throughout the investigation, the performance of the two DR states that lie precisely in the low drift regions is consistently different from the other four states. As such, the states from the DR method in the direction of lowest relative acceleration magnitude are termed Lowest Drift Regions (LDR) for increased clarity. Note that the deputy spacecraft legend used in Figure 8 is the same for each of the performance metrics, and as such will be excluded from subsequent figures.

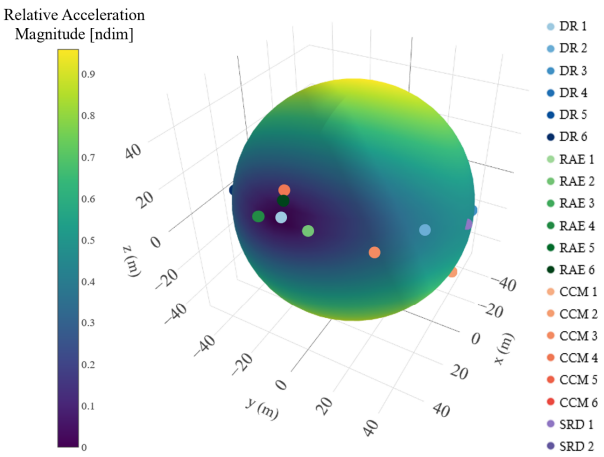

Figure 8: Deputy spacecraft initialization for Case 1 (TA = 170 degrees).

For many of the TAs tested, SRD locations align almost exactly in position space with the low drift region. This alignment ceases between 163 and 197 degrees TA, where the singular vector that has the most favorable predicted distance ratio switches. For basically all the loitering strategies at this short time horizon, there is symmetry across the x-z plane within the orbit, as expected due to the underlying symmetry within the

dynamics. This symmetry is only approximate for SRD states, which are dependent on dynamical information along the reference trajectory for the entire loitering time horizon. Figure 9 shows the result of numerical propagation of each deputy state, as viewed in a chief-centered rotating frame. It is clear that any drift of DR, RAE, and SRD spacecraft is slight, which is particularly true when starting near apolune. The CCM states move noticeably more, a characteristic of quasi-periodic behavior.

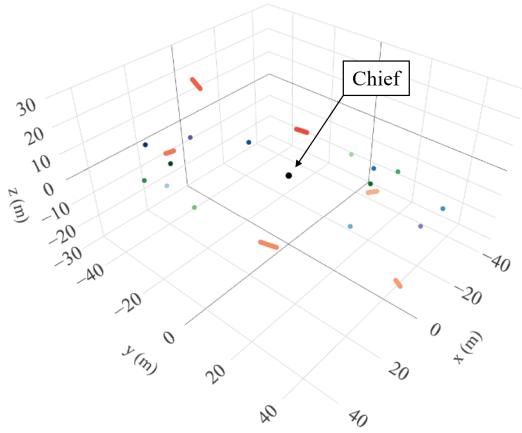

Figure 9: Deputy spacecraft relative motion for Case 1 (TA = 170 degrees).

Deputy spacecraft range to chief and inter-deputy range information is computed as a way to ensure that any method does not pose a risk to Gateway or other visiting vehicles. Figure 10 shows the spacecraft range to chief for the same TA of 170 and Figure 11 shows the distance between the two nearest deputy spacecraft for each strategy, ignoring spacecraft from any other strategy. With CCM states consistently moving much more than the other methods, the behavior is magnified in the figure for the DR, RAE, and SRD methods. Figure 10 highlights a key characteristic and limitation of the SRD implementation. The strategy is designed to target an initial-to-final distance ratio of approximately 1, which is accurate to within 5 cm for a majority of the TAs tested. However, due to the nature of the SVD, no guarantees can be made regarding the intermediate behavior. The behavior present in Figure 10 is common for this method, where the range changes during the loitering period, and then returns to approximately its original value at the final time. Comparatively, the better cases from the DR and RAE methods tend to hover around the desired range the entire time. Despite this fact, the final SRD range values are closest to the desired 50 meters for at least half of the TAs tested. As seen in Figure 11, the change in distances between deputy spacecraft is negligible at the current time horizon. For each TA tested, RAE spacecraft consistently have the lowest inter-deputy range due to how the states are tightly initialized on a contour line. While SRD has the highest distance, this is not a fair comparison due to the lower number of spacecraft simulated.

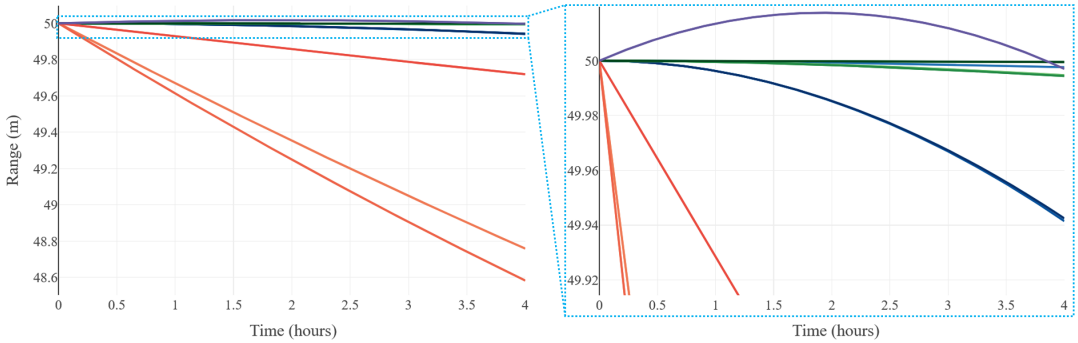

Figure 10: Deputy spacecraft range to chief spacecraft for Case 1 (TA = 170 degrees).

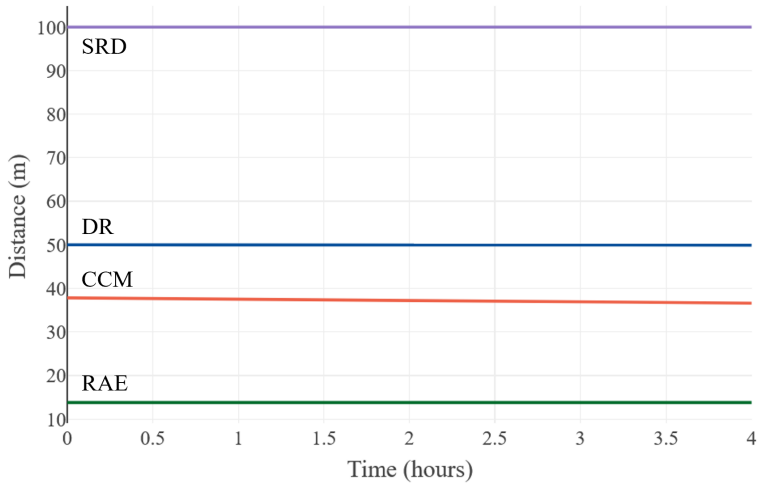

Figure 11: Range to nearest deputy for Case 1 (TA = 170 degrees).

At both ends of the TA domain, deputy range to chief changes more drastically and all spacecraft excluding those from the CCM method end closer to the chief than they began, at most by about 60 cm. Near apolune, these results vary based on the specific deputy spacecraft in question. CCM states generally contract toward the chief for TA values between 150 and 180, and expand for TA values between 180 and 210. While insightful, these quasi-periodic tendencies can be determined more directly by inspecting the geometry of the invariant torus of the corresponding QPO.

A leading goal of this investigation is to determine strategies that reduce the relative drift of the deputy spacecraft. The total drift magnitude for 170 degrees TA is visualized in Figure 12, as well as the in-line and transverse components of drift in Figure 13. Much of the same information is represented in the range to chief information as in the in-line drift, however the transverse drift yields additional insight into the motion. SRD states yield the least transverse drift for almost every simulation. This is most noticeable near the ends of the TA domain where all methods drift more due to increased nonlinear effects in the dynamics. The LDR states tend to have the most consistently low drift components at this time horizon, however the remaining four spacecraft in the DR method are among the highest drift. For the CCM states, drift is almost entirely transverse near apolune, with more comparable in-line components near the ends of the TA domain.

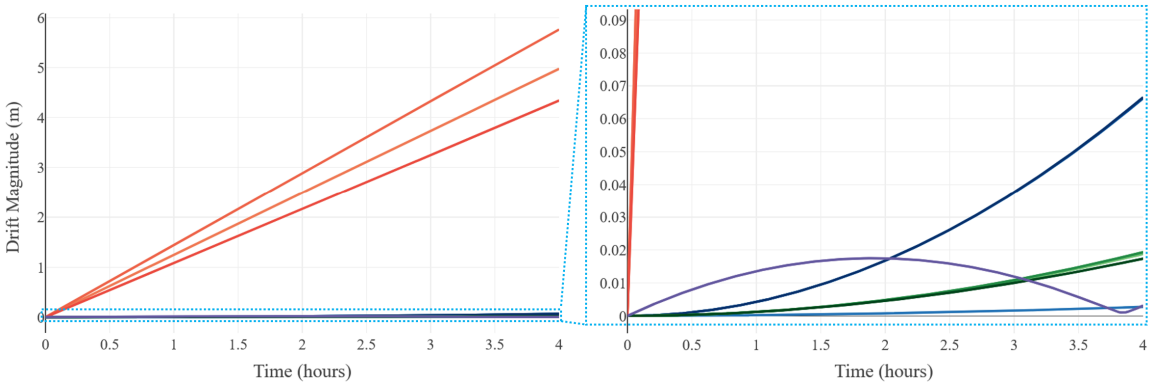

Figure 12: Deputy spacecraft total drift magnitude for Case 1 (TA = 170 degrees).

With respect to total drift, the best-performing strategies alternate between the LDR states and SRD states. For TAs of 150 to 162 and 197 to 210, SRD has the lowest drift at the final time, although not always in the intermediate times. For the rest of the TAs, SRD drift is slightly higher than LDR. Maximum drift

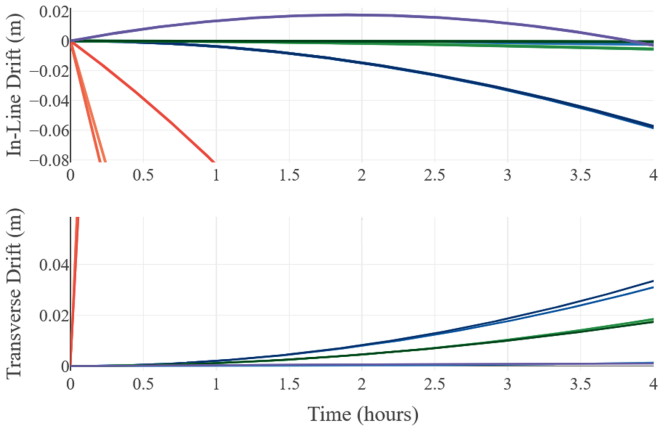

Figure 13: Deputy spacecraft drift components for Case 1 (TA = 170 degrees).

for all strategies excluding CCM states is roughly 65 cm overall, but stays below 10 cm for TAs in a 30 degree range surrounding apolune. It is also worth noting that SRD is the only strategy tested that does not monotonically increase in total drift magnitude throughout the loitering period. This is seen in Figure 12, where the spacecraft initially drifts by approximately 20 cm before returning toward its initial relative state at the final time. Contrarily, the drift magnitude of each other strategy strictly increases during every simulation. In Figure 14, range to chief information is summarized for the entire domain of TAs. For a given strategy, the smallest distance any deputy spacecraft reaches from the chief is reported as the worst case, and the largest closest approach is also recorded. The figure shows that behavior for the DR, RAE, and SRD methods varies significantly less than for the CCM states, and that the spread between best and worst cases is also diminished. Figure 15 shows information regarding the most and least drift magnitude at the final loitering time for each strategy, reinforcing many of the preceding observations. Notably, the figure highlights that SRD frequently ends closest to its initial relative state, which is particularly visible at the two ends of the TA domain. The highest drift of the three methods excluding CCM is consistently produced by the four DR states that do not begin in the regions of lowest relative acceleration magnitude.

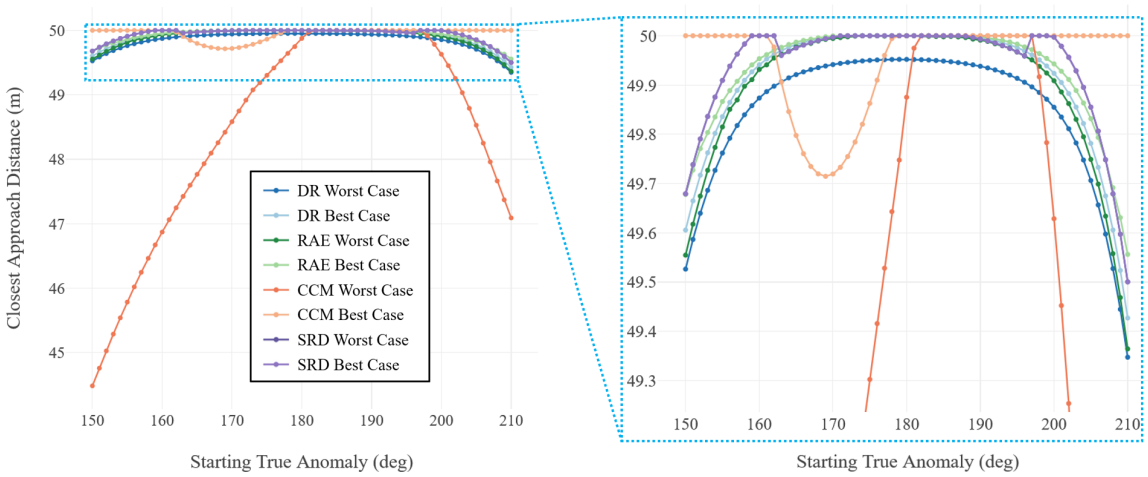

Figure 14: Deputy spacecraft closest approach distance versus TA for Case 1.

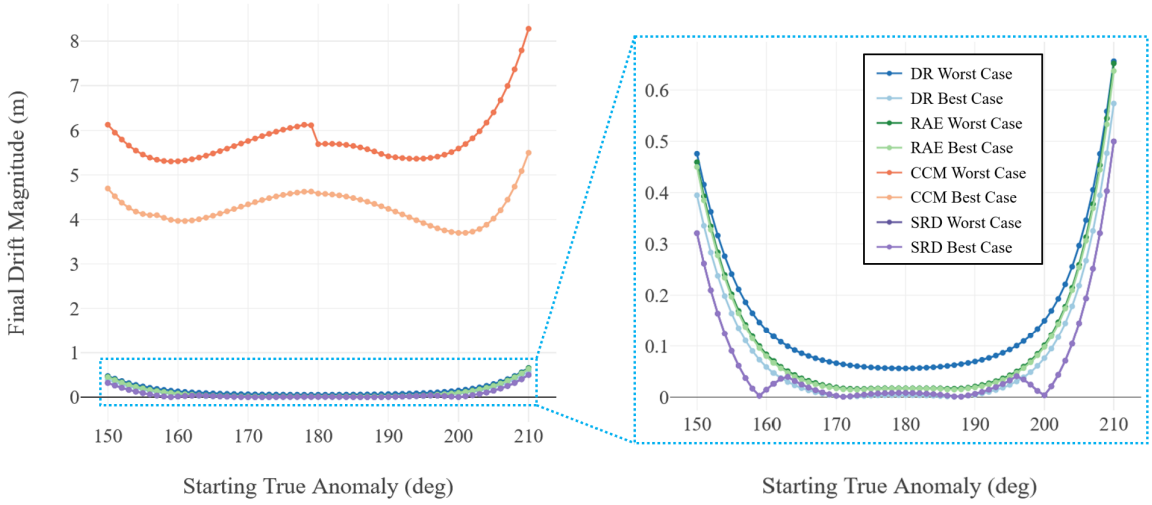

Figure 15: Deputy spacecraft final drift magnitude versus TA for Case 1.

CASE 2 RESULTS

Overall trends for Case 2 are presented in this section and a representative sample of performance outputs is provided for a TA of 194 degrees (ending at a TA of 204.86 degrees after 24 hours). Once again, deputy spacecraft are initialized and simulated for each TA in the range from 150 to 210 degrees, this time at a distance of 5 kilometers and for a loitering time horizon of 24 hours. Performance metrics are evaluated using deputy spacecraft states relative to the chief. Many of the observations from Case 1 persist into Case 2, with some key differences.

The initial spacecraft locations for the DR, RAE, and CCM methods are unchanged from Case 1 with the exception of the starting distance (and velocities scaled accordingly for CCM). Figure 16 shows the deputy spacecraft configurations for a TA of 194 degrees. The states for SRD are similar in location to Case 1, but now slightly more offset from the low drift region in position. The switch in direction that occurred in Case 1 is also present in Case 2, however beginning earlier at TA of 160 degrees. The noted symmetry about the x-z plane is still present in Case 2 with the exception of SRD states, which are now noticeably asymmetric about apolune. Figure 17 shows the relative motion of each deputy spacecraft with respect to the chief. In contrast to Case 1, the motion is visibly apparent, even near apolune.

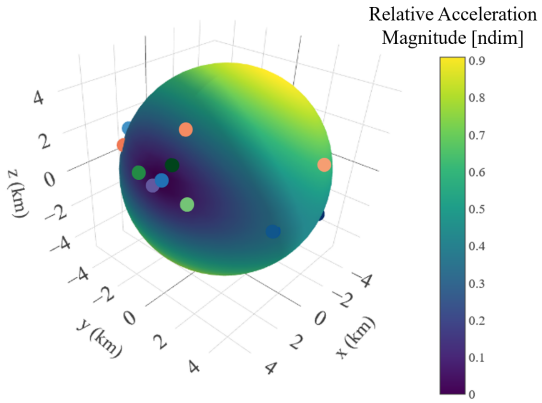

Figure 16: Deputy spacecraft initialization for Case 2 (TA = 194 degrees).

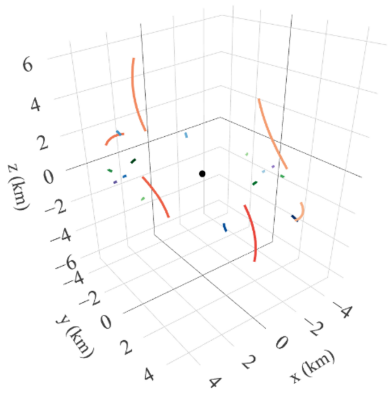

Figure 17: Deputy spacecraft relative motion for Case 2 (TA = 194 degrees).

Figures 18 and 19 show the range to chief and inter-deputy range information, respectively, for a TA of 194 degrees. Because the CCM motion overshadows the motion of other strategies and is better understood, the data in Figure 18 isolates the information for the remaining methods. This isolation of data is also employed for Case 2 drift information. The range to chief trends are generally the same as in Case 1, further exaggerated by the increased integration time. Toward the ends of the TA domain, deputy states in the DR, RAE, and SRD strategies tend to drift closer to the chief at the final time than they started, now by approximately a kilometer in the worst cases. Near apolune, DR and RAE closely maintain the desired range. As expected, the contraction and expansion characteristics of the CCM states are unchanged from Case 1. It is important to recognize that TA values past 204 degrees now reach perilune during their 24-hour time horizon. As a result, the domain of TA values that might be advantageous for proximity operations narrows with the higher loitering time to avoid complications near perilune. As illustrated in Figure 19, the distance between nearest deputy spacecraft begins to fluctuate more for the higher time horizon, however it remains benign for each of the strategies.

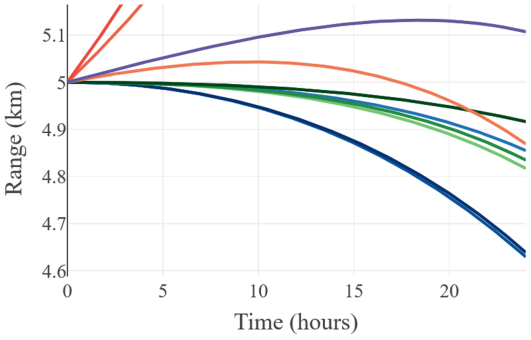

Figure 18: Deputy spacecraft range to chief spacecraft for Case 2 (TA = 194 degrees).

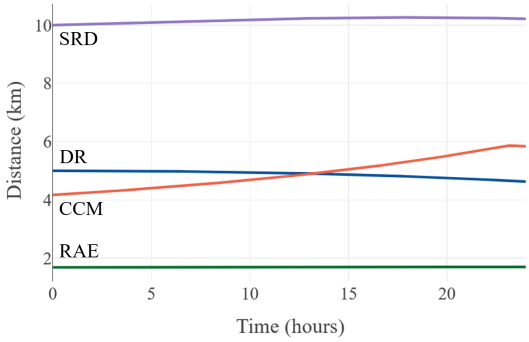

Figure 19: Range to nearest deputy for Case 2 (TA = 194 degrees).

Once again, the drift behavior presents the most insightful performance information for the loitering strategies. Figure 20 shows the drift components over time for a TA of 194 degrees, with overall drift magnitude provided in Figure 21. Trends are similar to Case 1 for each strategy. Notably, SRD is among the lowest transverse drift at the final time for all of the TAs tested and is often the lowest, particularly when the spacecraft begin to approach perilune. This can be seen in Figures 20 and 21 for 194 degrees TA, where the SRD states conclude the loitering phase with the lowest transverse and overall drift. However, the SRD characteristic behavior of intermediate drift prior to return is still present in Case 2, and is apparent in the total drift information.

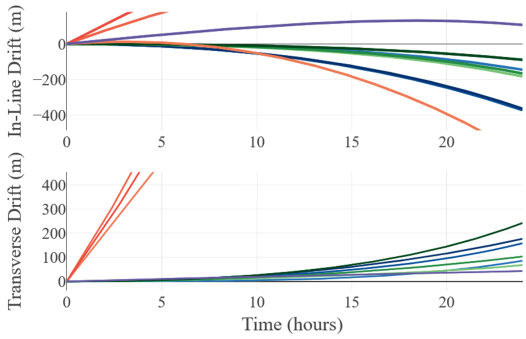

Figure 20: Deputy spacecraft drift components for Case 2 (TA = 194 degrees).

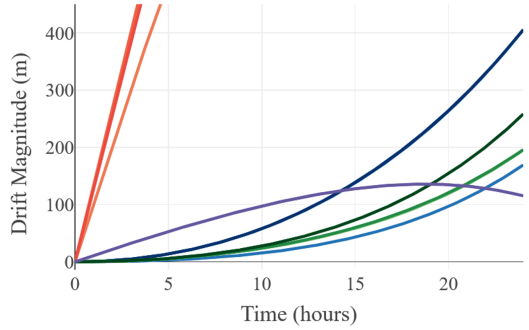

Figure 21: Deputy spacecraft total drift magnitude for Case 2 (TA = 194 degrees).

Near apolune, the two strategies with the consistently lowest overall drift are LDR and SRD. However, closer to the ends of the TA domain, SRD consistently yields lower drift, sometimes by over 200 meters at the final time. For this 24 hour loitering time, 4 distinct groups of drift behavior emerge. The lowest drift is consistently produced by the LDR and SRD strategies, as previously mentioned. RAE states exist together in a group of slightly higher total drift, followed by a grouping of the remaining DR states. Lastly, CCM states consistently yield the highest drift magnitudes and group together above the other methods. For the remaining three strategies, the maximum overall drift values are around 1 kilometer, excluding TAs that venture into the perilune region. For the 30 degrees TA centered around apolune, most states stay below 250 meters drift, with the better states typically below 50 meters. Consistent with Case 1, the only strategy for which the drift magnitude does not monotonically increase is SRD. Summary range and drift information across the domain of TA values is provided for Case 2 in Figures 22 and 23. Note that the sporadic behavior in both figures beginning around 205 degrees TA is due to the states approaching perilune near the end of the loitering simulation time.

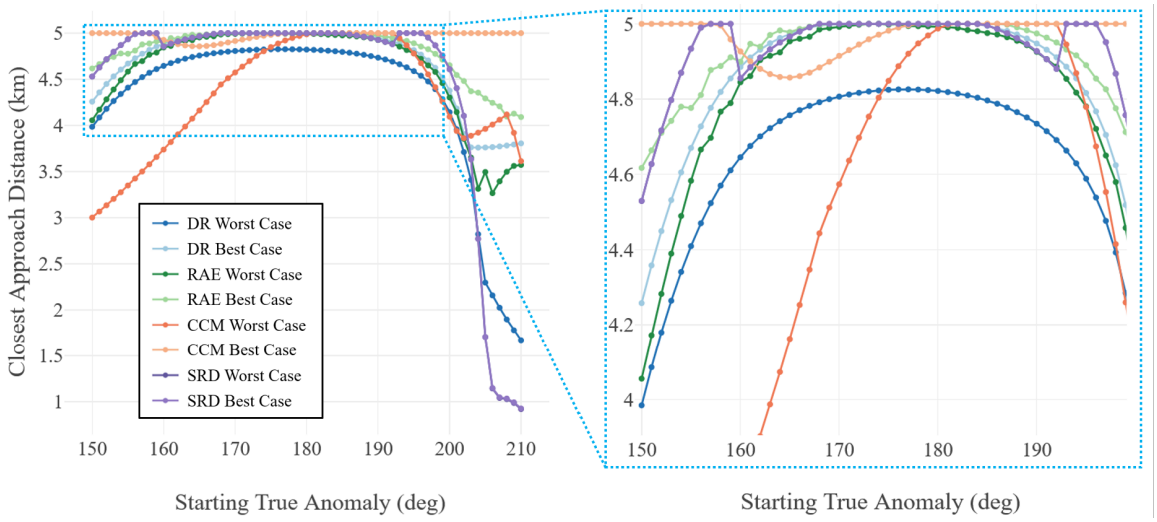

Figure 22: Deputy spacecraft closest approach distance versus TA for Case 2.

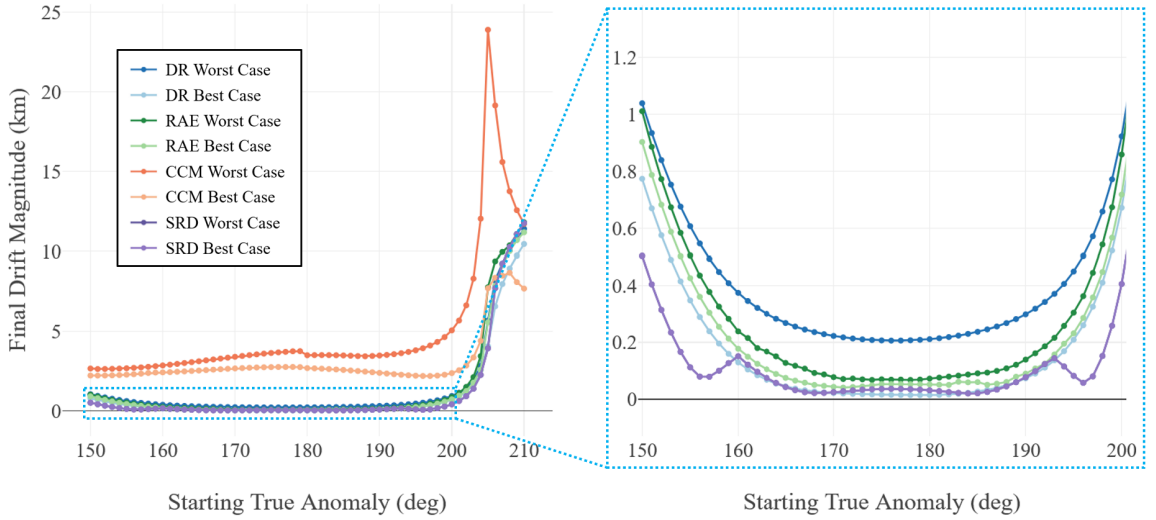

Figure 23: Deputy spacecraft final drift magnitude versus TA for Case 2.

FULL-PERIOD BEHAVIOR

For completeness, each strategy is also simulated for a full period of the underlying orbit and a separation distance of 5 kilometers to assess their behavior in the case that rendezvous or departure could not be performed. Figure 24 shows the relative motion of each deputy spacecraft for a starting TA of 166 degrees. It is clear from the figure that no strategies are able to maintain their relative position to any reasonable extent for the entire propagation. In general, all short-term trends observed in Cases 1 and 2 for the three methods excluding CCM break down as a result of passage through perilune. Alignment that occurs between the low drift regions and SRD states for short time horizons is nonexistent for longer simulations. The DR and RAE methods, which rely solely on dynamical information present at the initial time, possess erratic behavior beyond perilune.

While relative positions are mostly limited to their local neighborhood for the two short-term test cases, more of the 3D space surrounding the chief is occupied at some point during full-period simulations. CCM states, which approximate an invariant manifold, are consistently best behaved in the long-term. The SRD states also generally end close to the target range to chief, however the intermediate behavior is chaotic. The most alarming change observed for full-period behavior is captured in the range between spacecraft. Figure 25 shows the deputy spacecraft range to chief over the full period simulation starting at a TA of 166 degrees. In the simulation pictured, two of the RAE states dip to concerningly low ranges at perilune, around 110 hours into the simulation. The closest approach is within 180 meters of the chief spacecraft. Similarly for the inter-deputy range, there are cases where distances dropped below 80 meters for DR states. These cases of undesirable range are inconsistent and very dependent on the starting TA and deputy initial states, highlighting the variability of the DR, RAE, and SRD methods for passage through perilune.

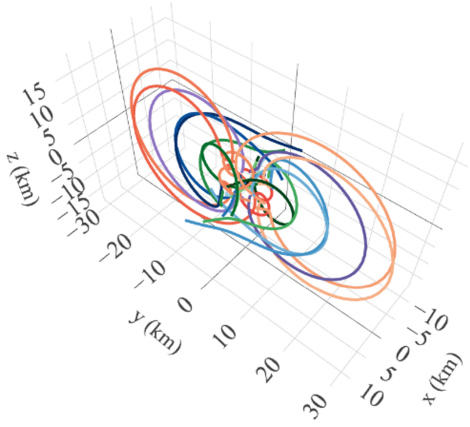

Figure 24: Deputy spacecraft relative motion for full NRHO period (TA = 166 degrees).

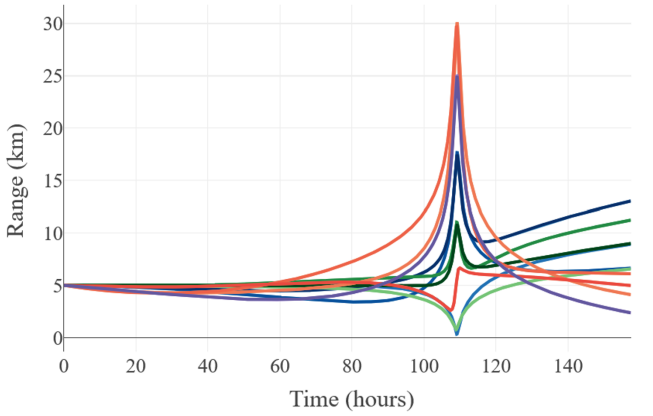

Figure 25: Deputy spacecraft range to chief spacecraft for full NRHO period (TA = 166 degrees).

FUTURE WORK

The analysis presented in this paper includes only a small sample of proposed formation flying techniques from literature and applies them to a spacecraft loitering scenario. It is likely that the incorporation of other proposed methods could prove to be useful and potentially illuminating to efficient RPOD practices in the cislunar regime and libration point orbits. The current investigation is limited to the CR3BP, which is a greatly simplified model of the governing dynamics. Each proposed method may be implemented within an ephemeris force model using the Gateway reference trajectory to obtain a more complete picture of performance for short-term loitering. Additionally, the SRD method is very limited in its scope due to the definition of states along one specific direction. The authors are currently investigating the formulation of relative states as a combination of these principal directions for loitering and rendezvous applications.

CONCLUDING REMARKS

Concepts proposed for formation flight in libration point orbits are implemented in a short-term spacecraft loitering application, demonstrating their potential utility for RPOD near the Gateway NRHO. For short-term loitering consistent with the time horizons tested, deputy states that match the chief spacecraft velocity and are offset by a small distance tend to maintain their relative position very closely near apolune. This is especially true when the relative position of the deputy is in a direction of low relative acceleration magnitude as determined from either the nonlinear equations of motion or the first-order variational equations. Apolune is shown to be the most efficient location to perform loitering, provided the goal is to reduce the relative drift of deputy spacecraft. This is due in part to the higher accuracy of the linear approximations near apolune, where the dynamics vary significantly more slowly. The domain of osculating true anomalies near apolune where proximity operations might be most efficient depends on the selected loitering time.

Throughout the analysis, there is no single, leading strategy, as the desired performance depends on the application. If the goal is to maintain a consistent relative position for the entire loitering period, the DR and RAE methods perform the most consistently. If the goal is to minimize the relative drift at the final time, the SRD method often performs the best. However, all three of these methods possess erratic behavior when the simulation includes passage through perilune. By comparison, CCM states are predictable and reliable for the entirety of the orbital period, which is much more beneficial for long-term loitering than maintaining a specific relative configuration. Each of the four strategies would benefit from further maturation. This is especially true for the SRD method, which is in a very preliminary conceptual stage and warrants further investigation due to its strong performance.

ACKNOWLEDGEMENTS

The authors wish to acknowledge support from the NASA SBIR (Small Business Innovative Research) program, as well as the technical insights provided by the Gateway Mission Design team at Johnson Space Center.

REFERENCES

[1] K. Johnson, "Fly Me to the Moon: Worldwide Cislunar and Lunar Missions," Feb, 2022. https://www.csis.org/analysis/fly-me-moon-worldwide-cislunar-and-lunar-missions.

[2] D. Connell, "Gateway," Jan, 2024. https://www.nasa.gov/mission/gateway/.

[3] D. C. Davis, S. T. Scheuerle, D. A. Williams, F. S. Miguel, E. M. Zimovan-Spreen, and K. C. Howell, "Orbit Maintenance Burn Details for Spacecraft in a Near Rectilinear Halo Orbit," *2022 AAS/AIAA Astrodynamics Specialists Conference*, Charlotte, North Carolina, August, 2022.

[4] S. T. Scheuerle, D. C. Davis, E. M. Zimovan-Spreen, B. P. McCarthy, D. B. Henry, and K. C. Howell, "Jettison and Disposal from Near Rectilinear Halo Orbits, Part 1: Theory," *AAS/AIAA Astrodynamics Specialist Conference*, Big Sky, Montana, August, 2023.

[5] D. C. Davis, E. M. Zimovan-Spreen, S. T. Scheuerle, and K. C. Howell, "Debris Avoidance and Phase Change Maneuvers in Near Rectilinear Halo Orbits," *44th Annual AAS Guidance, Navigation, and Control Conference*, Breckenridge, Colorado, February, 2022.

[6] W. H. Clohessy and R. S. Wiltshire, "Terminal Guidance System for Satellite Rendezvous," Vol. 27, No. 9, pp. 653–658. Publisher: American Institute of Aeronautics and Astronautics.

[7] W. Fehse, *Automated Rendezvous and Docking of Spacecraft*. Cambridge: Cambridge University Press, 2003.

[8] Barden, B. T. and Howell, K. C., "Fundamental Motions Near Collinear Libration Points and Their Transitions," *The Journal of the Astronautical Sciences*, Vol. 46, 1998, pp. 361–378.

[9] Howell, K. C. and Pernicka, H. J., "Numerical Determination of Lissajous Trajectories in the Restricted Three-Body Problem," *Celestial Mechanics*, Vol. 41, 1988, pp. 107–124.

[10] B. G. Marchand and K. C. Howell, "Control Strategies for Formation Flight In the Vicinity of the Libration Points," *Journal of Guidance, Control, and Dynamics*, Vol. 28, 2005, pp. 1210–1219.

[11] F. Y. Hsiao and D. J. Scheeres, "The Dynamics of Formation Flight About a Stable Trajectory," *Journal of the Astronautical Sciences*, Vol. 50, 2002, pp. 269–287.

[12] S. Cuevas del Valle, H. Urrutxua, P. Solano-López, R. Gutierrez-Ramon, and A. K. Sugihara, "Relative Dynamics and Modern Control Strategies for Rendezvous in Libration Point Orbits," *Aerospace*, Vol. 9, 2022, p. 798.

[13] Elliott, Ian and Bosanac, Natasha, "Describing relative motion near periodic orbits via local toroidal coordinates," *Celestial Mechanics and Dynamical Astronomy*, Vol. 134, 2022, p. 19.

[14] Franzini, Giovanni and Innocenti, Mario, "Relative Motion Dynamics in the Restricted Three-Body Problem," *Journal of Spacecraft and Rockets*, Vol. 56, 2019, pp. 1322–1337.

[15] D. Zuehlke, A. Sizemore, and T. Henderson, "(Preprint) AAS 23-112 Periodic Relative Natural Motion in the Circular Restricted Three-Body Problem," *33rd AAS/AIAA Space Flight Mechanics Meeting*, Austin, Texas, January, 2023.

[16] S. D'Amico, A. Koenig, B. Macintosh, and S. Mall, "System Design of the Miniaturized Distributed Occulter/Telescope (mDOT) Science Mission," *33rd Annual AIAA/USU Conference on Small Satellites*, Logan, Utah, August, 2019.

[17] "European Space Agency – About Proba-3," 2024. https://www.esa.int/Enabling_Support/Space_Engineering_Technology/Proba_Missions/About_Proba-3.

[18] Heritier, Aurelie and Howell, Kathleen, "Dynamical evolution of natural formations in libration point orbits in a multi-body regime," *Acta Astronautica*, Vol. 102, 2014, pp. 332–340.

[19] B. McCarthy, *Cislunar Trajectory Design Methodologies Incorporating Quasi-Periodic Structures With Applications*. Ph.D. Dissertation, Purdue University, West Lafayette, Indiana, 2022.

[20] Farquhar, Robert W. and Kamel, Ahmed A., "Quasi-periodic orbits about the translunar libration point," *Celestial mechanics*, Vol. 7, 1973, pp. 458–473.

[21] Gómez, G. and Masdemont, J. and Simó, C., "Quasihalo Orbits Associated with Libration Points," *The Journal of the Astronautical Sciences*, Vol. 46, 1998, pp. 135–176.

[22] Z. Olikara, *Computation of Quasi-Periodic Tori and Heteroclinic Connections in Astrodynamics Using Collocation Techniques*. Ph.D. Dissertation, University of Colorado, Boulder, Boulder, Colorado, 2016.

[23] N. Baresi, *Spacecraft Formation Flight on Quasi-periodic Invariant Tori*. Ph.D. Dissertation, University of Colorado, Boulder, Boulder, Colorado, 2017.

[24] Henry, Damennick and Scheeres, D., "Expansion Maps: Designing Relative Trajectories on Quasi-Periodic Orbits," *Journal of Guidance, Control, and Dynamics*, Vol. 44, 2020, pp. 457–468.

[25] V. Muralidharan, *Stretching Directions in Cislunar Space: Stationkeeping and an Application to Transfer Trajectory Design*. Ph.D. Dissertation, Purdue University, West Lafayette, Indiana, 2021.

[26] Short, Cody R. and Blazevski, Daniel and Howell, Kathleen C. and Haller, George, "Stretching in phase space and applications in general nonautonomous multi-body problems," *Celestial Mechanics and Dynamical Astronomy*, Vol. 122, 2015, pp. 213–238.

[27] Muralidharan, Vivek and Howell, Kathleen C., "Stretching directions in cislunar space," *Astrodynamics*, Vol. 7, 2023, pp. 153–178.

[28] R. Whitley and R. Martinez, "Options for Staging Orbits in Cis-Lunar Space," *IEEE Annual Aerospace Conference*, Big Sky, Montana, October, 2015.

[29] M. Gupta, K. C. Howell, and C. Frueh, "Constellation Design to Support Cislunar Surveillance Leveraging Sidereal Resonant Orbits," *33rd AAS/AIAA Space Flight Mechanics Meeting*, Austin, Texas, January, 2023.